Appl. Phys. A (2014) 117:2133–2141
DOI 10.1007/s00339-014-8633-7

Applied Physics A
Materials Science & Processing

Molecular dynamics study of the short laser pulse ablation: quality and efficiency in production

D. S. Ivanov · V. P. Lipp · V. P. Veiko · E. Yakovlev · B. Rethfeld · M. E. Garcia

Received: 11 July 2014 / Accepted: 15 July 2014 / Published online: 2 August 2014

Abstract The ablation mechanism of solids due to a short laser pulse energy deposition is a complex phenomenon, which depends on both the laser input parameters and the material properties. In particular, when moving toward pico-second and even femto-second pulses, the irradiated material can be driven to extreme conditions, when its properties are not strictly defined and a number of transient inter-related processes determining a further material's evolution are occurring simultaneously on the nanoscale. Some of the processes were successfully studied experimentally and resulted in numerous publications. The difficulties of the experimental measurements, however, and often the impossibility to isolate those processes for their detailed study, make theoretical investigation beneficial. Here, we are targeting the determination of the working ablation regimes in technological terms of quality and production. The utilized atomistic–continuum model combines the advantages of the molecular dynamics method in description of the laser-induced non-equilibrium phase transition processes at atomic level with the ability of the two temperature model in the continuum description of the photo-excited free carrier's dynamics. On the example of Al and Au metal targets, the model is applied to study the ablation regimes induced with laser irradiation of different fluences and pulse durations. The obtained photo-thermal and photo-mechanical modes are related with quality and production terms from the point of industrial applications.

D. S. Ivanov (✉) · V. P. Lipp · B. Rethfeld
Technical University of Kaiserslautern and OPTIMAS Research Center, Kaiserslautern, Germany
e-mail: ivanov@uni-kassel.de

D. S. Ivanov · V. P. Veiko · E. Yakovlev
Saint-Petersburg National Research University of Information Technologies, Mechanics and Optics, Saint Petersburg, Russia

D. S. Ivanov · V. P. Lipp · M. E. Garcia
University of Kassel, Kassel, Germany

1 Introduction

Short laser pulse ablation is a widely used phenomenon in a number of industrial applications. The possibility to deposit a large amount of energy into a very localized volume with short laser pulses has been proven as an efficient tool in short laser pulse drilling, cutting, and welding experiments [1–3]. The resulting features, however, especially from the point of their quality appeared to be a strong function of laser irradiation parameters. For instance, it was shown experimentally and theoretically that both the electron–phonon coupling strength and the pulse duration can play an important role in the laser damage mechanism [4, 5]. According to these works, the character of damage in target's evolution, including processes of melting, spallation, evaporation, and ablation in general, is essentially determined by the question whether the pulse duration is long or short as compared to the characteristic electron–phonon relaxation time. In other works, the material properties were assumed also as important for the characterization of the final structures [6, 7]. Thus, in a number of experiments, two clearly distinguished modes in the ablation rate have been found at low and high fluencies for some materials such as Au and Ag [8, 9]. The corresponding low and high ablation rates, as they scaled with the applied fluence, were suggested to originate from the fact that either regimes of thermal or stress confinement is dominant, and whether the resulting damage and its quality is achieved due to photo-thermal or photo-mechanical mechanism accordingly [10, 11].

Theoretical calculations with molecular dynamics (MD)-based approach provided similar observations and figured out that the photo-mechanical and photo-thermal regimes are related to quality and production. In particular, the conditions of inertial stress confinement, realized in short pulse laser-matter experiments, have been identified as a main driving mechanism for the onset of spallation, which bears mechanical character of the incurred damage rather than thermal one [12, 13]. In this case, the observed material removal depth was greater, which is the indicator of the ablation efficiency, whereas the induced thermal damage of the new generated surfaces was minimized, which is the indicator of the ablation quality. The corresponding condition of the laser heating to attain such the regime was suggested in the following relation [14, 15]:

$$\max\left\{\tau_{\text{pulse}}, \tau_{\text{e-ph}}\right\} \approx \tau_{\text{heating}} \leq \tau_{\text{mech}} \approx \frac{L_{\text{e-diff}}}{C_s} \quad (1)$$

where the characteristic mechanical relaxation time, τ_{mech}, due to internal stresses occurs to be greater than the heating time, τ_{heating}, which is determined by either the pulse duration, τ_{pulse}, or the characteristic electron–phonon relaxation time, $\tau_{\text{e-ph}}$, whichever is greater. The mechanical relaxation time, on the other hand, is a function of the effective depth of the laser energy deposition, $L_{\text{e-diff}}$, and the speed of sound in the material, C_s.

Providing appropriate conditions for the onset of the spallation mechanism, however, Eq. (1), due to uncertain value of $L_{\text{e-diff}}$, is barely applicable in the material processing prediction, if speaking about efficiency and quality. There are two essential mechanisms of the laser-deposited energy channelization in the material: the fast electron heat conduction due to hot electrons, determining the depth of the energy deposition, and the electron–phonon energy exchange, determining the rate of lattice heating [16]. Their inter-relation as a function of the irradiation parameters together with the materials properties was in particular considered with the help of two temperature model (TTM) [17, 18] in a recent simplified theoretical approach [14]. But what is more important, the material properties such as the electron heat conduction, electron heat capacity, and the strength of the electron–phonon energy coupling are functions of the electron temperature [17, 19, 20]. Here, we neglect the possible dependence on the electron distribution [13, 21, 22]. Figure 1a and b show that the strength of the electron–phonon coupling is increasing with the electronic temperature for both metals. For Au material, this increase is more pronounced due to significant d-band electrons contribution. The variations in the electron heat conductivity functions for both materials are more different. Due to a much greater Fermi temperature (135,000 K) of the Al material, its conductivity linearly scales with the electronic temperature at least up to 30,000 K, whereas for Au material, possessing relatively low Fermi temperature (56,000 K), the conductivity mechanism is strongly influenced by the electron–electron collisions already at 20,000 K that leads to decay of the conductivity function, resulting in the onset of thermal confinement. The electron temperature dynamics, in turn, is strongly affected by the pulse duration and the applied fluence. Therefore, with such complex dependencies of the material properties on the electron temperatures, we can consequently achieve one or another working ablation regime or mixture of them for the same material depending on the irradiation parameters.

In the present theoretical research, we are trying to clarify the validity and applicability of the previously made estimations, given by Eq. (1), in order to isolate these regimes and attain the optimization of the laser parameters to find optimal working modes in the industrial applications for short laser pulse materials processing.

2 The model

Targeting our research aim, we use a hybrid atomistic–continuum model that has been proven as an effective numerical tool in the microscopic analysis of non-equilibrium phase transition processes during an ultra-short laser pulse interaction with thin and thick metal targets [5, 12, 13]. The idea of hybrid modeling is based on the ability of the MD approach to track down the kinetics of ultra-fast laser-induced processes in the solid at atomic level on one hand, and the continuum description of free photo-excited carrier's dynamics with the help of TTM model on the other hand. In the combined MD–TTM model, the equation for lattice temperature in TTM is completely substituted with the MD equations of motion, and the energy exchange between lattice and hot electrons is accounted for in the MD part via an additional frictional term. The detailed description of the MD–TTM model can be found elsewhere [5, 23]. The parameterization of the interatomic potential, however, has been shifted to Zhakhovskii's representation [24] due to its more accurate representation of material properties as they are given by the experiment. The constructed model, therefore, apart from the inherent kinetics at the atomic scale, is capable of describing the laser light absorption, fast electron heat conduction, strong laser-generated electron–phonon non-equilibrium, and can be applied to study short pulse laser-induced processes including melting, vaporization, spallation, and ablation [25].

To fulfill our investigation tasks, we chose two very different metal representatives: Al and Au that belong to the so-called transitional and noble metallic groups, respectively, with relatively short and long electron–phonon relaxation

times respectively. Their values are in general functions of the excitation parameters, but for the chosen materials and under similar irradiation conditions, they differ at least by one order of magnitude. Under moderate conditions, reproduced in our calculations, the corresponding relaxation times averaged over the time of electron–phonon equilibration process can be roughly estimated as ~ 1 ps for Al and ~ 20 ps for Au [4, 14, 26]. The MD–TTM computational cell for both Al and Au samples consists of $20 \times 20 \times 400$ lattice units in *X*-, *Y*-, and *Z*-axis, respectively, accounting for 640,000 atoms in total. Consequently, with the lattice parameters of 0.406 nm for Al and 0.408 nm for Au, the MD part of the constructed computational cells is representing a film of about 160 nm thickness with lateral sizes of the MD cell of about 5 nm. However, if dynamically behaving pressure-transmitting boundary conditions are applied at the bottom of the MD part [27], we can assume our targets as thick, as it was demonstrated in recent works [28]. The continuum part of the combined model provides the heat flow drainage away from the excited volume to a distance of more than 20 μm. The thickness of the MD part, however, must obey the conditions of no phase transition occurring deeper than the non-reflective boundaries, which is fulfilled for all the simulations presented in this paper. The computational setup is divided into approximately 1-nm unit cells that leaves high enough spatial resolution for the TTM part of the model and still satisfies the size of the statistical ensemble for a reliable determination of thermo-physical properties determination in the MD part (such as temperature, pressure, and density), which are averaged over neighboring cells accounting, therefore, for about 4,000 particles. Finally, we apply free boundary conditions atop of the sample for its exposition to a laser pulse and periodic boundary conditions in the directions perpendicular to the laser pulse propagation (*X* and *Y*).

3 Results

In order to show the difference in the evolution between two chosen materials following laser excitation, we expose the Al target to 0.2 and 6.0 ps pulses and Au target to 6.0 and 60 ps pulses. Thus, in both cases, we have the laser pulse well below and well above the characteristic electron–phonon relaxation time. Moreover, according to the behavior of the conductivity function with the electronic temperature, specifically for Au, two limiting cases from the point of the effective laser energy deposition depth are expected, see Fig. 1: the heat confinement in the vicinity of the material surface due to suppressed conduction process and a strong increase of the energy deposition depth at high degrees of excitation. Sequentially, the materials will be exposed to the laser irradiation at different absorbed fluences in order to identify different working modes from the point of damage mechanism.

We begin with a simple case of the laser ablation of an Al target. Since this material has a characteristic electron–phonon relaxation time of only ~ 1 ps, the incident pulse

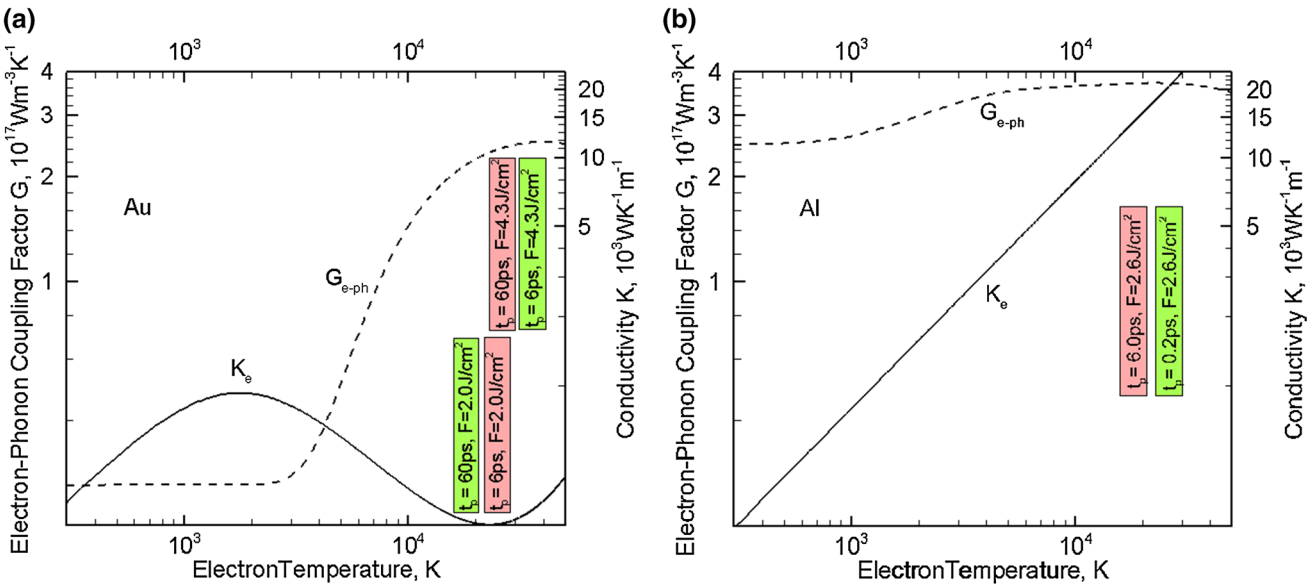

Fig. 1 Conductivity (*solid*) and the electron–phonon coupling (*dashed*) for Au (**a**) and Al (**b**) materials as function of the electron temperatures [17, 19, 20] at constant lattice temperature of 300 K. The *rectangles* indicate the laser parameters applied in the productive simulations discussed in the Results section. The *areas* they cover in *horizontal direction* (electron temperature axis) roughly correspond to the ranges of electron temperature change during the processes of most active laser-deposited energy dissipation. The *green* and *red color* correspondingly refer to the better or poor efficiency of the material removal and the quality of the final damage (see text)

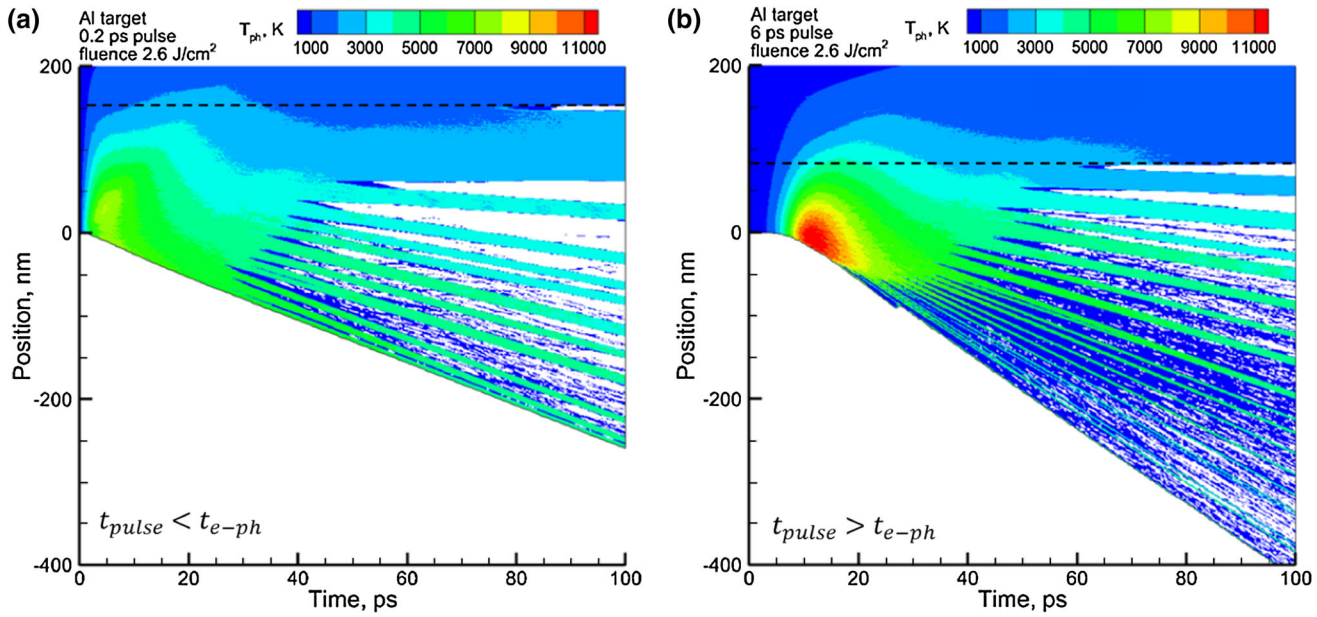

Fig. 2 Lattice temperature contour plots of the 0.2 ps (**a**) and 6 ps (**b**) pulse interaction with a thick Al target at an absorbed fluence of 2.6 J/cm^2. *Dashed line* is the maximum spallation depth

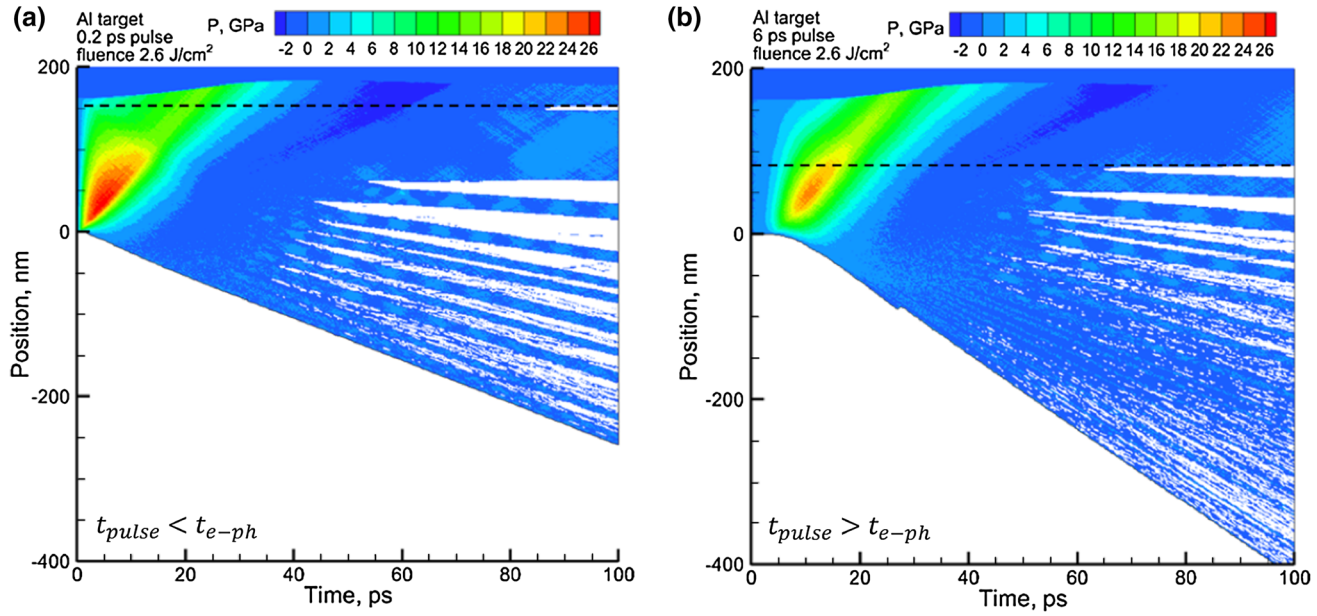

Fig. 3 Pressure contour plots of the 0.2 ps (**a**) and 6 ps (**b**) pulse interaction with a thick Al target at an absorbed fluence of 2.6 J/cm^2. *Dashed line* is the maximum spallation depth

of 0.2 ps can be considered as short, whereas the pulse of 6.0 ps is accepted as a long one. The results of these pulse interactions with the Al sample are presented as contour plots of lattice temperature and pressure in Figs. 2 and 3 for the short (a) and long (b) pulses, respectively. One can see that they are notably different for the same absorbed fluence.

The interpretation of these calculations can be assisted with Fig. 1b, where the functions of electron conductivity and electron–phonon coupling strength for Al material are plotted with respect to electronic temperature. In particular, the short pulse induces a higher electronic temperature ($\sim$30,000 K), Fig. 1b green rectangle, which in turn results in the higher value of the conductivity function. Therefore, in case of the shorter pulse, the effective energy deposition proceeds to a greater distance on which the temperature and pressure gradients are established with lower value of the temperature in the surface region,

as compared to the longer pulse. Furthermore, for the pulse duration shorter than the electron–phonon relaxation time, the material has no sufficient time for thermal expansion in response to its fast heating. The formation of high internal stresses, therefore, is trapped within the solid that leads to the so-called conditions of the inertial stress confinement, usually characterized by high internal stresses and relatively low temperature established over $L_{\text{e-diff}}$ distance. As a result, the relaxation of internal stresses will proceed as an unloading pressure wave that run across the material and can cause its rupture (spallation) at a certain depth (or in several places), where tensile stresses are strong enough at the given lattice temperature. This kind of damage is related to the photo-mechanical one and apparently is more desirable from the point of efficiency (ablation rate), due to deeper rapture development, and from the point of quality (clean material removal), since less thermal damage of the surrounding material parts. This can be justified when comparing the results depicted in Figs. 2 and 3. The maximum depth where spallation (ablation) occurred is indicated by a dashed line here and on all following contour plots. One can see, therefore, that the maximum ablation depth per pulse is greater for the shorter pulse, and at the same time, the damage is bearing less thermal character.

A different situation is seen when considering 6.0 ps pulse interacting with the same sample at the same absorbed fluence. Since the pulse is long in this case, the highest generated electronic temperature due to low laser pulse intensity will be relatively smaller ($\sim$20,000 K), that in turn keeps the conductivity function values lower as well, Fig. 1a red rectangle. As a result, the temperature and pressure gradients are formed on a shallower depth as compared to the previous case and the conditions of inertial stress confinement are not fulfilled here, or at least, do not play a dominant role. Instead, the higher temperature spawning over shorter depth results rather in the establishment of conditions of thermal confinement. In this regime, the relaxation of internal stresses running across pre-surface regions results in active splashing of the molten material leading to a lower spallation depth, a lot more vapor and much more serious thermal damage in the remaining material than it is in case of the mechanical one, see Figs. 2a and 3a. Apparently, Figs. 2b and 3b show a poor working mode in industrial applications from the point of efficiency and quality.

Next, we consider the 6.0- and 60-ps laser pulse interactions with Au material at the absorbed fluence of 2.0 J/cm^2. Since the characteristic electron–phonon relaxation time of Au is about 20 ps, the former pulse is now considered as short, whereas the latter is a long one. The results of these calculations are presented in Figs. 4 and 5 as contour plots of lattice temperature and pressure. From the first glance, we do not observe anyhow similar results with that we have just had on Al material. These results can be interpreted, however, if we carefully consider the ranges of the electronic temperatures achieved this time for both pulses in relation with the conductivity and the electron–phonon coupling strength function of Au, Fig. 1a. One can see that although significant stresses are developing within

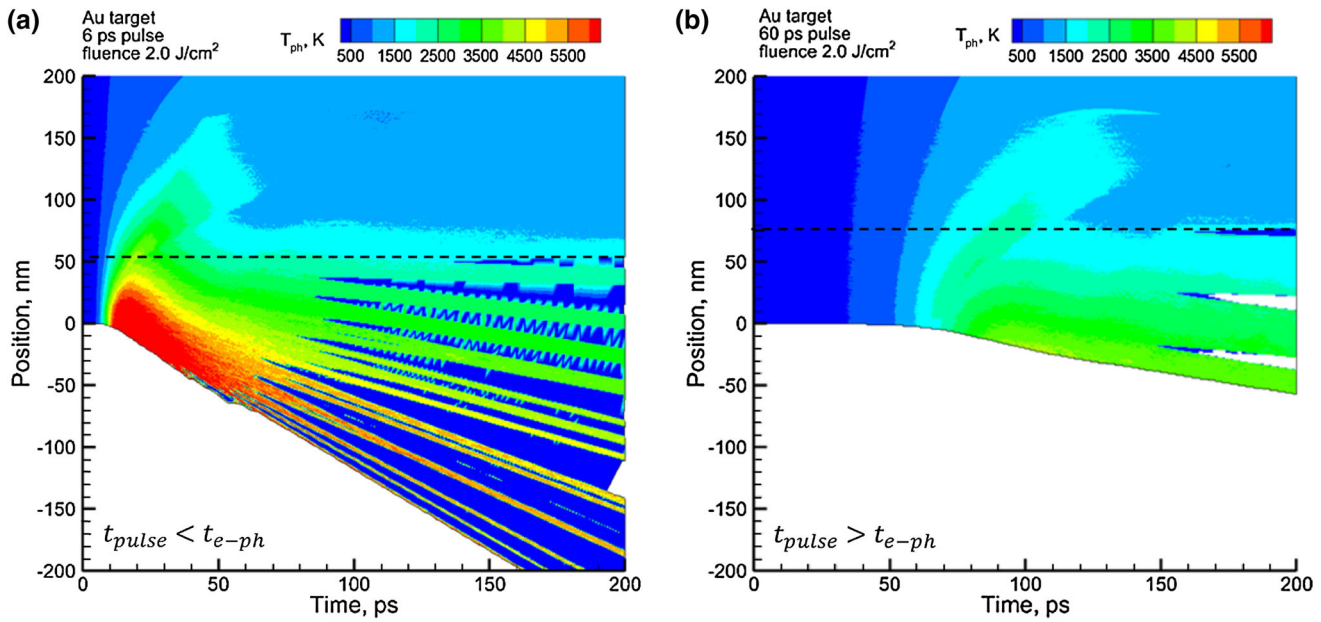

Fig. 4 Lattice temperature contour plots of the 6.0 ps (**a**) and 60 ps (**b**) pulse interaction with a thick Au target at an absorbed fluence of 2.0 J/cm^2. *Dashed line* is the maximum spallation depth. The *blue fields* between spalled layers in (**a**) indicate volumes containing small clusters, i.e., droplets rather than vapor

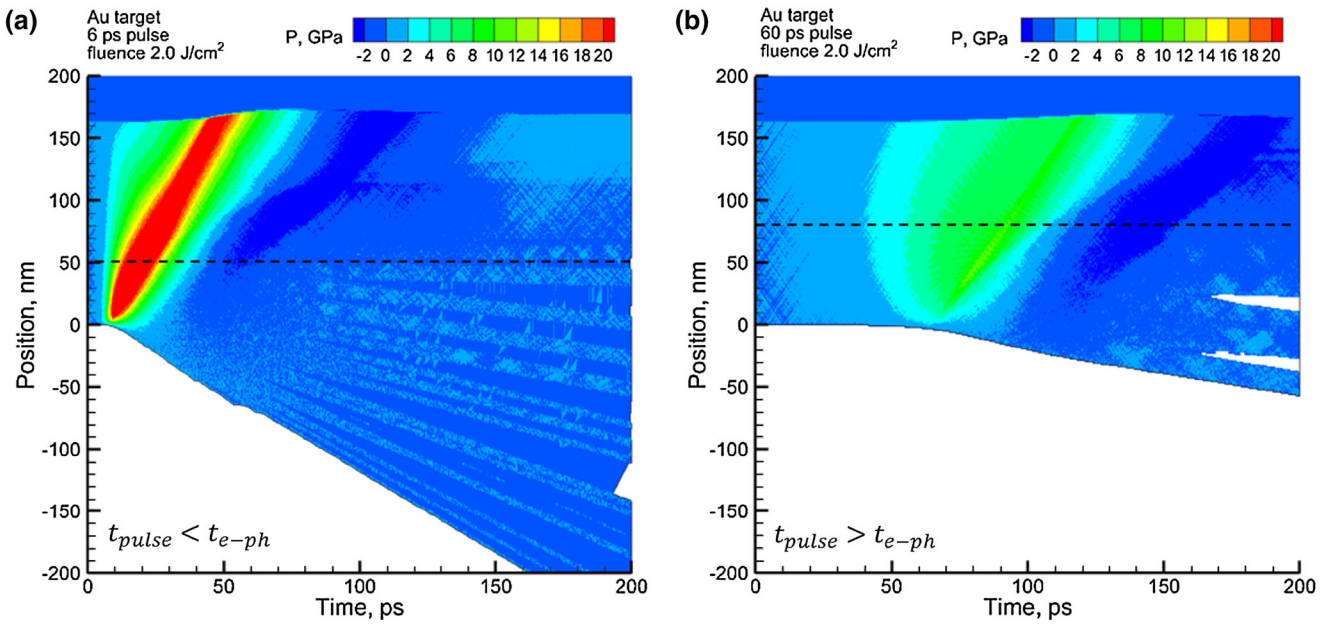

Fig. 5 Pressure contour plots of the 6.0 ps (**a**) and 60 ps (**b**) pulse interaction with a thick Au target at an absorbed fluence of 2.0 J/cm^2. *Dashed line* is the maximum spallation depth. The *blue fields* between spalled layers in (**a**) indicate volumes containing small clusters, i.e., droplets rather than vapor

the surface area as a result of fast heating, the shorter pulse at the given fluence leads rather to the conditions of the thermal confinement, Figs. 4a and 5a. The induced electronic temperatures (30,000 K) due to electron–electron collisional processes result in decay of the conductivity function with simultaneous increase of the electron–phonon coupling strength due to d-band excitation, which physically means high lattice temperature at a limited laser energy deposition depth, L_{e-ph}, Fig. 1a, red lower rectangle. The relaxation of the internal stresses over shorter L_{e-ph} distance results in active splashing of the molten phase and significant thermal damage of the sample. Note that under the applied laser parameters, the short laser pulse results in even smaller material removal depth as compared with the long one, which technologically means a smaller ablation rate. The 60-ps pulse, although inducing lower electronic temperatures (20,000 K), results in higher values of the conductivity function and yet lower strength of the electron–phonon coupling, Fig. 1a, lower green rectangle. Despite the fact that, according to Eq. (1), the conditions of inertial stress confinement are not fulfilled in this modeling, the more active laser-deposited energy dissipation via conductivity channel results in not significant thermal damage of the irradiated target and even a bit deeper onset of the spallation, as compared to the character of damage incurred in the case of the shorter pulse, Figs. 4b and 5b.

The situation changes, however, with the absorbed fluence increased up to 4.3 J/cm^2, Figs. 6 and 7. The same pulse durations this time induce higher electronic temperatures (correspondingly 30,000 K in case of 60 ps pulse and 40,000 K in case of 6.0 ps one), which in turn bring the conductivity function of Au into the plasma-like scaling regime for the shorter pulse, Fig. 1b upper green rectangle, whereas the longer one leaves it at the lower values, Fig. 1a upper red rectangle. Meanwhile, the strength of electron–phonon coupling is approximately same in both cases. The intensive laser-deposited energy dissipation via the conductivity process along with strong heating due to electron–phonon coupling results in the inertial stress confinement regime playing a dominant role. A much deeper onset of the spallation mechanism for the short pulse indicates the photo-mechanical character of the target damage with high production rate and quality, Figs. 6a and 7a. On the other hand, the long pulse does not trigger the development of high internal stresses and leads to the thermal-confinement regime that results in photo-thermal damage of the irradiated sample with low production rate and poor quality, Figs. 6b and 7b.

4 Discussion and conclusion

To summarize our research, we can finally generalize the formulation of the inertial stress confinement regime suggested by Eq. (1) and, utilizing the relation $G_{e-ph} \sim C_e/\tau_{e-ph}$ [17] over the electron–phonon equilibration period, expand this expression in the following way:

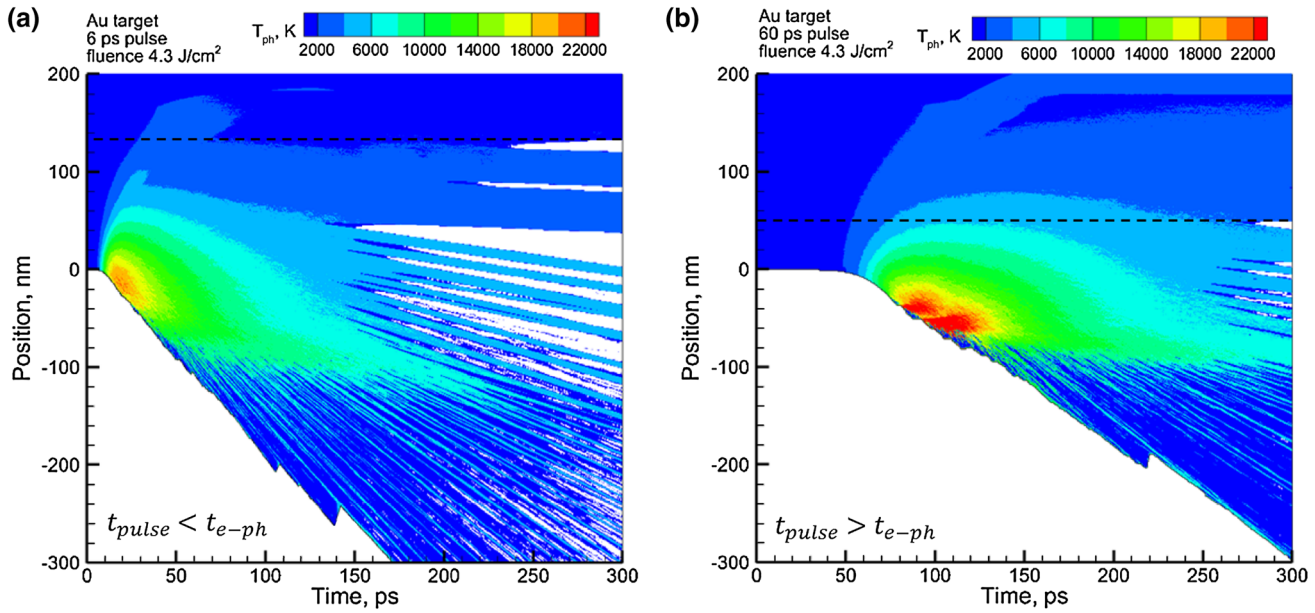

Fig. 6 Lattice temperature contour plots of the 6.0 ps (**a**) and 60 ps (**b**) pulse interaction with a thick Au target at an absorbed fluence of 4.3 J/cm^2. *Dashed line* is the maximum spallation depth

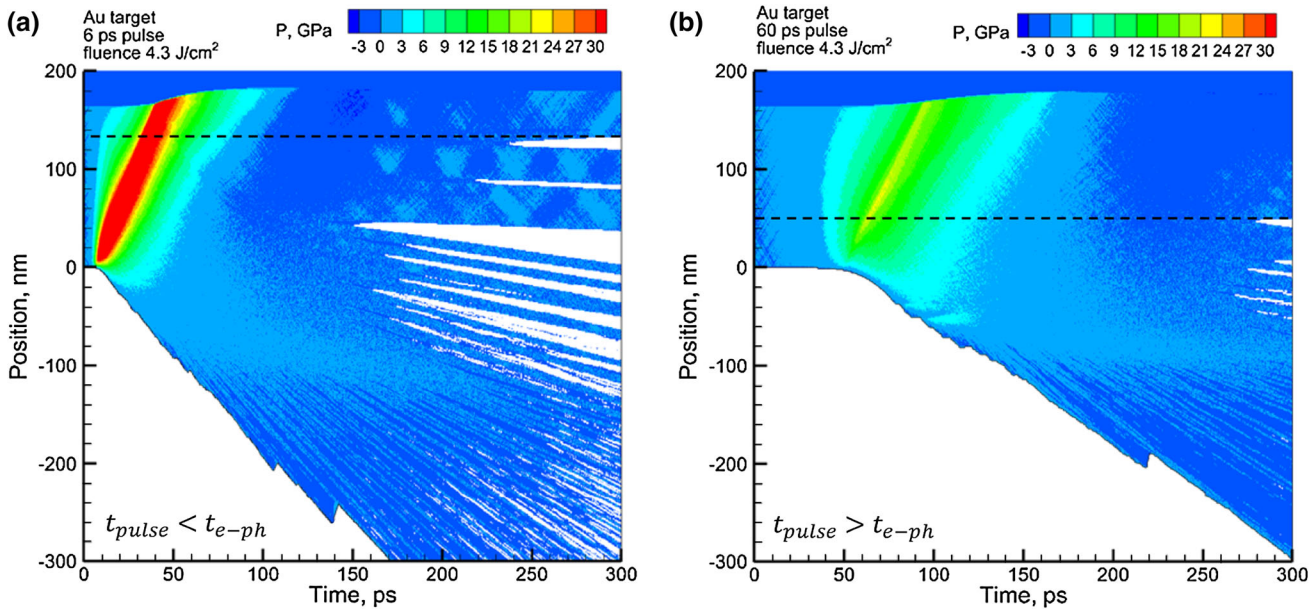

Fig. 7 Pressure contour plots of the 6.0 ps (**a**) and 60 ps (**b**) pulse interaction with a thick Au target at an absorbed fluence of 4.3 J/cm^2. *Dashed line* is the maximum spallation depth

$$\max\left\{\tau_{\text{pulse}}, \tau_{\text{e-ph}}\right\} \approx \tau_{\text{heating}} \le \tau_{\text{mech}} \approx \frac{L_{\text{e-diff}}}{C_{\text{s}}} \approx \frac{\sqrt{D_{\text{e}}\tau_{\text{e-ph}}}}{C_{\text{s}}} = \frac{\sqrt{\tau_{\text{e-ph}} k_{\text{e}}(F_{\text{las}})/C_{\text{e}}(F_{\text{las}})}}{C_{\text{s}}} \approx \frac{\sqrt{k_{\text{e}}(F_{\text{las}})/G_{\text{e-ph}}(F_{\text{las}})}}{C_{\text{s}}} \quad (2)$$

where D_{e}, k_{e}, $G_{\text{e-ph}}$, and C_{e} are the electron diffusivity, the electron heat conductivity, the electron–phonon coupling, and the electron heat capacity functions correspondingly. At the given pulse duration, τ_{pulse}, they all depend on the electronic temperature, the characteristic values of which (achieved upon laser energy absorption and essentially affecting the temperature-dependent parameters) in turn are defined by the applied laser fluence, F_{las}. It now becomes clear that in order to achieve high efficiency and quality regime in the production lines involving the ablation phenomena, one has to minimize the left side of the inequality

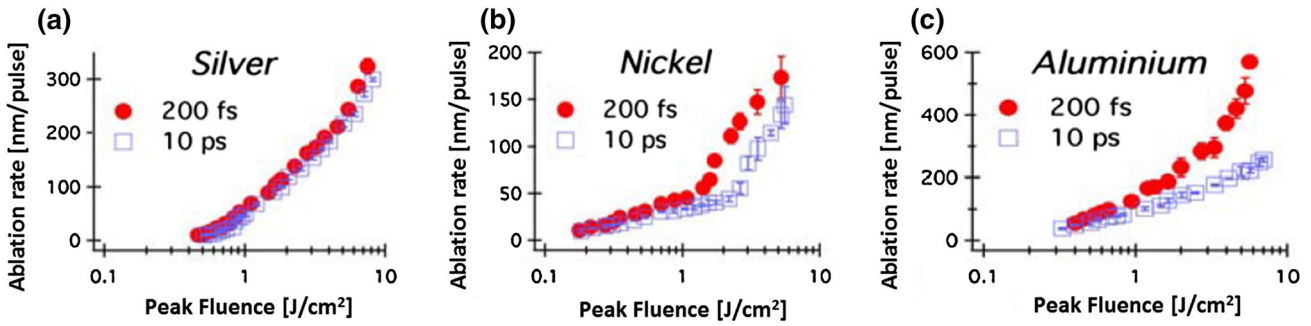

Fig. 8 Experimentally measured ablation rates of the selected materials Ag (**a**), Ni (**b**), and Al (**c**) versus absorbed fluence for pulse durations of 0.2 ps (*circles*) and 10 ps (*squares*) [9]

by simply shortening the pulse (below the electron–phonon relaxation time) and maximize the right side of the inequality by means of playing with the applied fluence in regards with the material properties, as they are depicted in Fig. 1.

The suggested theory fits very well to the data, obtained in the experimental works [8–10], and replotted here, Fig. 8. In that research [9], two applied pulse durations were short, moderate, or long depending on the properties of material under ablation process. Both pulses, 0.2 and 10 ps are short for Ag material and the ablation rate exposes the more or less linear behavior with fluence indicating the photo-mechanical character of the damage mechanism due to realization of the inertial stress confinement conditions. For Al material, 10-ps pulse is a long one. Therefore, the conditions of inertial stress confinement will not be realized even at high fluences. Its damage mechanism, therefore, will expose the photo-thermal character, whereas the short 200-fs pulse will trigger the photo-mechanical one. Finally, the Ni material with the characteristic electron–phonon relaxation time of about 10 ps is a bordering case so that both characters of the damage mechanisms are involved. Depending on the applied fluence, photo-mechanical or photo-thermal mechanism will be in play or a mixture of them.

The deduced formula also correlates with our recent theoretical calculations [14], where laser-deposited energy channelization interplays between the electron–phonon collisions and the electron heat conduction were considered from the point of optimal pulse duration for achieving the maximal temperature on the material's surface upon the laser irradiation. The interplay between those two channels of laser-deposited energy dissipation is also reflected in Eq. (2). One can see that, regardless the pulse duration, the stronger the electron–phonon energy exchange function $G_{\text{e–ph}}$ and the smaller the values of the conductivity function K_{e}, the shallower effective depth of the laser energy deposition $L_{\text{e-diff}}$, and the higher temperature will be achieved at the material's surface as a result. However, as Eq. (2) shows, this situation is the indication of thermal-confinement regime, not desirable in the industrial applications in general.

Finally, it is also necessary to mention that depending on the particular material properties and even on the applied model to simulate them, the obtained results can slightly vary in determination of the working ablation regimes. For example, the effect of surface roughness and polycrystallinity of the irradiated target, considered in [15], can increase the range of the photo-mechanical damage zone, whereas a more sophisticated model on electron thermal conductivity discussed in [20] or the model on the electron–phonon coupling function presented in [19], can slightly decrease it. Anyway, the essential message of this paper is that for the given pulse duration, shorter than the electron–phonon relaxation time, there exists such a fluence range, where due to strong scaling of the thermal conductivity function with the induced electron temperature, one can achieve a laser energy deposition depth sufficient for the onset of the inertial stress confinement regime. The latter leads to the high production rate with simultaneously sharp quality in technological applications of short laser pulse machining of solids.

Acknowledgments The presented work is completed under financial support due to Russian Federation Government grant 074-U01, the Leading State Universities of Russian Federation subsidy NSH 1364.2014.2, and DFG grant IV 122/1, and RE 1141/14.

References

1. F.P. Mezzapesa, T. Sibillano, L.L. Columbo, F. Di Niso, A. Ancona, M. Dabbicco, F. De Lucia, P.M. Lugarà, G. Scamarcio, Direct investigation of the ablation rate evolution during laser drilling of high aspect ratio micro-holes. in *Laser Applications in Microelectronic and Optoelectronic Manufacturing XVII SPIE Proceedings,* vol. 8243, p. 7 (2012)
2. S. Lo Turco, G. Nava, R. Osellame, K.C. Vishnubhatla, R. Ramponia, Femtosecond laser micromachining for optofluidic and energy applications. Opt. Mat. **36**, 102 (2013)

3. N.H. Rizvi, Femtosecond laser micromachining: current status and applications. in *Laser Precision Microfabrication RIKEN Review*, vol. 50 (2003)
4. S.-S. Wellershoff, J. Hohlfeld, J. Gudde, E. Matthias, The role of electron–phonon coupling in femtosecond laser damage of metals. Appl. Phys. A **69**, S99 (1999)
5. D.S. Ivanov, L.V. Zhigilei, Combined atomistic–continuum modelling of short-pulse laser melting and disintegration of metal films. Phys. Rev. B **68**, 064114 (2003)
6. H. Huang, L.-M. Yang, J. Liu, Micro-hole drilling with femtosecond fiber laser. in *Proceedings of SPIE Photonics West 201*, vol. 8607, p. 19 (2013)
7. P. Simon, J. Ihlemann, Machining of submicron structures on metals and semiconductors by ultrashort UV-laser pulses. Appl. Phys. A **63**, 505 (1996)
8. S. Nolte, C. Momma, H. Jacobs, A. Tunnemann, B.N. Chichkov, B. Wellegehausen, H. Welling, Ablation of metals by ultrashort laser pulses. J. Opt. Soc. Am. B **14**, 2716 (1997)
9. P.T. Mannion, S.F. Favre, D.S. Ivanov, G.M. O'Connor, T.J. Glynn, J.G. Lunney, B. Doggett, Langmuir probe investigation of plasma expansion in femto- and picosecond laser ablation of selected metals. J. Phys: Conf. Ser. **59**, 753 (2007)
10. C. Momma, S. Nolte, B.N. Chichkov, F.V. Alvensleben, A. Tunnerbaum, Precise laser ablation with ultrashort pulses. Appl. Surf. Sci. **109/110**, 15 (1997)
11. H.K. Toenshoff, A. Ostendorf, S. Nolte, F. Korte, T. Bauer, *Micro-machining using femtosecond lasers*, ed. by S. Miyamoto, K. Sugioka, T.W. Sigmon. Proceedings of SPIE, First International Symposium on Laser Precision Microfabrication, vol. 4088, p. 136 (2000)
12. E. Leveugle, D.S. Ivanov, L.V. Zhigilei, Photochemical spallation of molecular and metal targets: molecular dynamic study. Appl. Phys. A **79**, 1643–1655 (2004)
13. L.V. Zhigilei, Z. Lin, D.S. Ivanov, Atomistic modeling of short pulse laser ablation of metals: connections between melting, spallation, and phase explosion. J. Chem. Phys. **113**, 11892 (2009)
14. D.S. Ivanov, B.C. Rethfeld, The effect of pulse duration on the character of laser heating: photo-mechanical vs. photo-thermal damage of metal targets. Appl. Surf. Sci. **255**, 9724 (2009)
15. D.S. Ivanov, V.P. Lipp, B. Rethfeld, M.E. Garcia, Molecular-dynamics study of the mechanism of short-pulse laser ablation of single-crystal and polycrystalline metallic targets. J. Opt. Technol. **81**, 250 (2014)
16. L.V. Zhigilei, D.S. Ivanov, Channels of energy redistribution in short-pulse laser interactions with metal targets. Appl. Surf. Sci. **248**, 433 (2005)
17. S.I. Anisimov, B.L. Kapeliovich, T.L. Perel'man, Electron emission from metal surfaces exposed to ultrashort laser pulses. Zh. Eksp. Teor. Fiz. **66**, 776 (1974) [Sov. Phys. JETP **39**, 375 (1974)]
18. S.I. Anisimov and B. Rethfeld, On the theory of ultrashort laser pulse interaction with metals. in *Proceedings of SPIE International Society for Optical Engineering* (*USA*), vol. 3093, p. 192 (2002)
19. Z. Lin, L.V. Zhigilei, V. Celli, Electron–phonon coupling and electron heat capacity of metals under conditions of strong electron–phonon nonequilibrium. Phys. Rev. B **77**, 075133 (2008)
20. M.E. Povarnitsyn, N.E. Andreev, E.M. Apfelbaum, T.E. Itina, K.V. Khishchenko, O.F. Kostenko, P.R. Levashov, M.E. Veysman, A wide-range model for simulation of pump–probe experiments with metals. Appl. Sur. Sci. **258**, 9480 (2012)
21. B.Y. Mueller, B. Rethfeld, Relaxation dynamics in laser-excited metals under nonequilibrium conditions. Phys. Rev. B **87**, 035139 (2013)
22. B.Y. Mueller, B. Rethfeld, Nonequilibrium electron–phonon coupling after ultrashort laser excitation of gold. Appl. Surf. Sci. **302**, 24 (2014)
23. D.S. Ivanov, A.I. Kuznetsov, V.P. Lipp, B. Rethfeld, B.N. Chichkov, M.E. Garcia, W. Schulz, Short laser pulse surface nanostructuring on thin metal films: direct comparison of molecular dynamics modeling and experiment. Appl. Phys. A **111**, 675 (2013)
24. V.V. Zhakhovskii, N.A. Inogamov, Y.V. Petrov, S.I. Ashitkov, K. Nishihara, Molecular dynamics simulation of femtosecond ablation and spallation with different interatomic potentials. Appl. Surf. Sci. **255**, 9592 (2009)
25. Ch. Wu, L.V. Zhigilei, Microscopic mechanism of laser spallation and ablation of metal targets from large-scale molecular dynamics simulations. Appl. Phys. A **114**, 11 (2014)
26. J.B. Lee, K. Kang, S.H. Lee, Comparison of theoretical models of electron–phonon coupling in thin gold films irradiated by femtosecond pulse lasers. Mater. Trans. **52**, 547 (2011)
27. C. Schäfer, H.M. Urbassek, L.V. Zhigilei, B.J. Garrison, Pressure-transmitting boundary conditions for molecular dynamics simulations. Comput. Mater. Sci. **24**, 421 (2002)
28. L.V. Zhigilei, D.S. Ivanov, E. Leveugle, B. Sadigh, E.M. Bringa, Computer modeling of laser melting and spallation of metal targets. in *Proceedings of SPIE High Power Laser Ablation V*, vol. 5448, p. 505 (2004)